

EXPERIMENTAL STUDY OF DRACS THERMAL PERFORMANCE IN A LOW-TEMPERATURE TEST FACILITY

Q. Lv, H.C. Lin, X. Sun, R.N. Christensen, and T.E. Blue

Nuclear Engineering Program, The Ohio State University
201 W. 19th Avenue, Columbus, OH 43210, USA
lv.11@osu.edu; sun.200@osu.edu

G. Yoder and D. Wilson

Oak Ridge National Laboratory
P.O. Box 2008, Oak Ridge, TN 37831, USA
yodergljr@ornl.gov; wilsondf@ornl.gov

P. Sabharwall

Idaho National Laboratory
1955 N. Fremont Avenue, Idaho Falls, ID 83415, USA
Piyush.sabharwall@inl.gov

ABSTRACT

Direct Reactor Auxiliary Cooling System (DRACS) is a passive decay heat removal system proposed for the Fluoride-salt-cooled High-temperature Reactor (FHR) that combines coated particle fuel and a graphite moderator with a liquid fluoride salt as the coolant. The DRACS features three coupled natural circulation/convection loops, relying completely on buoyancy as the driving force. These loops are coupled through two heat exchangers, namely, the DRACS heat exchanger and the natural draft heat exchanger. To experimentally investigate the thermal performance of the DRACS, a scaled-down low-temperature DRACS test facility (LTDF) has been constructed. The design of the LTDF is obtained through a detailed scaling analysis based on a 200-kW prototypic DRACS design developed at The Ohio State University. The LTDF has a nominal power capacity of 6 kW. It uses 1.0-MPa water as the primary coolant, 0.1-MPa water as the secondary coolant, and ambient air as the ultimate heat sink. Two accident scenarios simulated in the LTDF are discussed in this paper. In the first scenario, the DRACS startup scenario occurs with no initial flow in either the LTDF primary or secondary loop, and the system is launched from a cold state. In the second scenario, a reactor coolant pump trip process is studied, during which a flow reversal phenomenon in the DRACS primary loop occurs. In both scenarios, natural circulation flows are developed as the transients approach to their quasi steady states.

KEYWORDS

FHR, DRACS, passive safety, decay heat removal

1. INTRODUCTION

Fluoride-salt-cooled High-temperature Reactors (FHRs) are an emerging reactor class that draws on four proven nuclear technologies, namely, the liquid salt of the molten salt reactors (MSRs), the coated particle fuel (TRISO particles) of high-temperature gas-cooled reactors (HTGRs), the pool configuration and passive safety system of the sodium-cooled fast reactors (SFRs), and Brayton power cycle technology [1,

2]. With the excellent heat transfer properties of the liquid fluoride salts, the FHRs possess several potential benefits, including increased design margins, high operation temperature and low operation pressure, high core power density, and improved decay heat removal capability [3].

The Direct Reactor Auxiliary Cooling System (DRACS), as shown schematically in Fig. 1, is a passive decay heat removal system proposed for FHRs. It features three coupled natural circulation/convection loops, relying on buoyancy as the driving force. The DRACS Heat Exchanger (DHX) that is submerged in the reactor primary coolant pool provides the coupling between the primary coolant and the DRACS secondary loop, while the Natural Draft Heat Exchanger (NDHX) couples the DRACS secondary loop with the ambient air. One important component that has been proposed to preserve the passive feature of the DRACS is a fluidic diode in its primary loop. Fluidic diodes are passive flow control devices with low flow resistance in one flow direction and high flow resistance in the opposite direction. The fluidic diode is orientated in such a way that during reactor normal operation, the primary salt flow into the DRACS DHX is restricted, thus preventing excessive heat loss to the DRACS. However, when the DRACS is functioning during reactor accidents, the primary salt flow is in the forward flow direction of the diode, i.e., downward as shown in Fig. 1 that features low flow resistance.

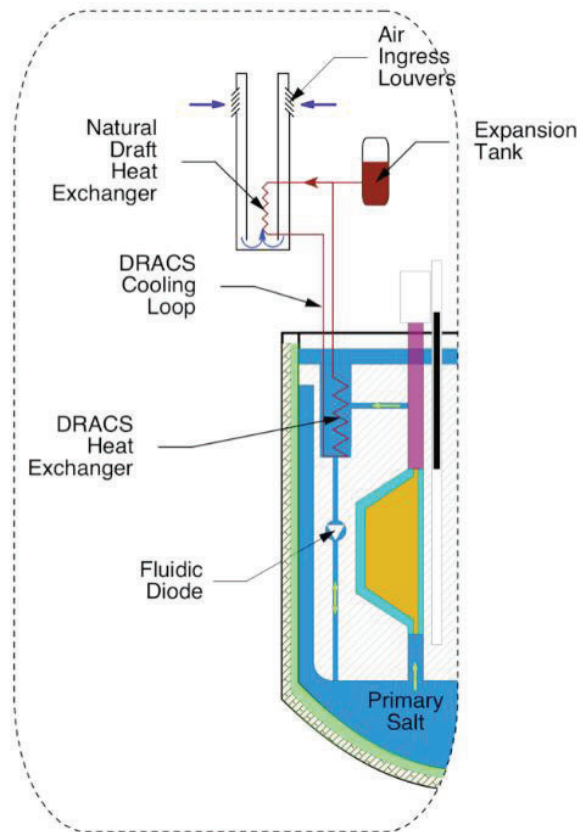


Figure 1. Schematic of the DRACS [4]

The concept of the DRACS originated from Experimental Breeder Reactor-II (EBR-II), and had been widely adopted in many existing pool type Sodium-cooled Fast Reactor (SFR) designs, e.g., EFR and KALIMER-600 [5]. The feasibility of the DRACS concept was demonstrated with two representative tests carried out in EBR-II in 1986. In the first test, loss of flow was initiated without scram from full

power. The second test was a loss of heat sink without scram from full power. Both tests demonstrated that natural processes, such as natural convection of the primary coolant and heat conduction, were able to keep the core cooled without causing any failure [5].

Although the technologies involved in FHRs have been proven in different preceding reactor designs, no complete FHR class design has yet been developed. It is proposed that the first FHR would necessarily be a test-scale reactor to validate the system attributes before proceeding to larger and commercial systems [4]. Recently, the Massachusetts Institute of Technology (MIT), University of California, Berkeley (UCB) and the University of Wisconsin Madison (UW) were developing a test-scale FHR design that could be deployed in the near future under an Integrated Research Project (IRP) sponsored by the U.S. Department of Energy [6]. This test-scale FHR features a thermal power smaller than 20 MWth. DRACS, as the passive decay heat removal system, should also be tested for its integral thermal performance in this test-scale FHR. Currently, efforts of designing, testing, and modeling the DRACS for a 20-MWth FHR are being carried out at The Ohio State University (OSU) independent of the IRP effort [7-11]. A modular prototypic DRACS design that is capable of removing 1% of the nominal core power, i.e., 200 kW, has been proposed [7, 10]. This prototypic design features a total height of 15 m, and would be challenging to be accommodated in a laboratory testing environment. Following the recently performed scaling analysis [9, 10], two scaled-down test facilities (low-temperature and high-temperature DRACS test facilities) were designed. The low-temperature facility is currently in operation while the high-temperature facility is under construction at OSU.

In this paper, two accident scenarios simulated in the low-temperature DRACS test facility (LTDF) are discussed. The first scenario simulates the DRACS startup with no initial flow in either the DRACS primary or secondary loop and without involvement of the reactor coolant pump. In the second scenario, the phenomenon of flow reversal in the DRACS primary loop is studied by tripping the reactor coolant pump following a long-term steady-state normal operation of the simulated reactor core. In both scenarios, natural circulations are successfully established, demonstrating the decay heat removal capability of the DRACS concept. In the pump trip scenario, the primary flow is found to reverse in about three seconds after the pump trip, and it takes much less time to reach a steady state than in the startup scenario.

2. LOW-TEMPERATURE DRACS TEST FACILITY

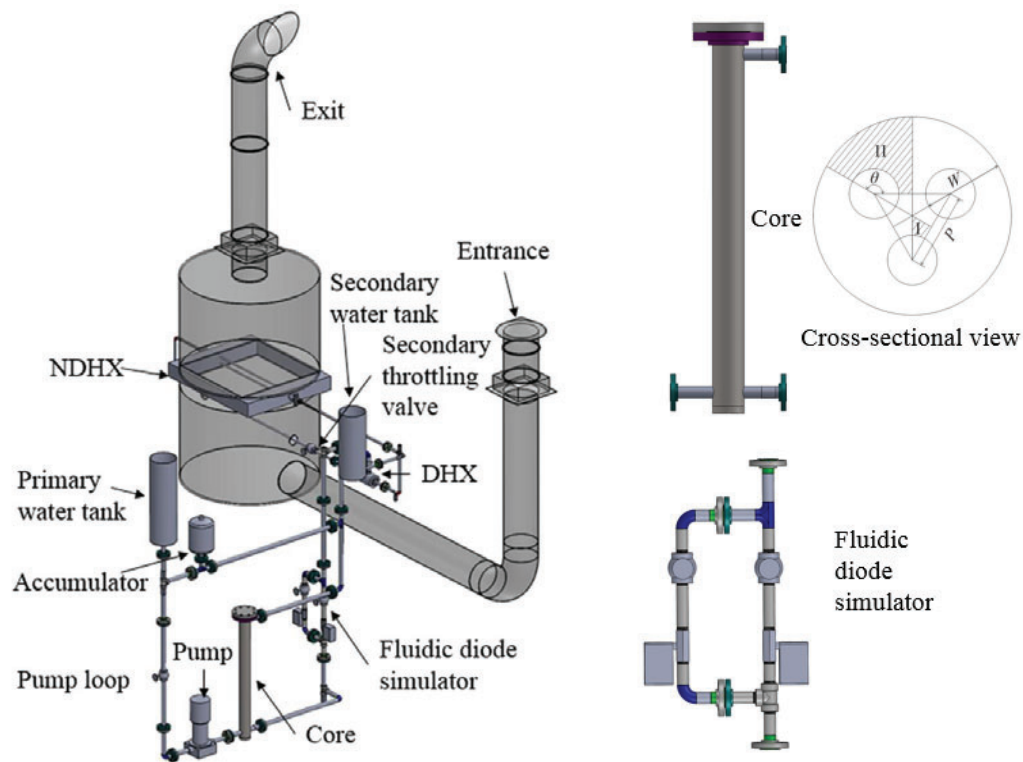
Following a rigorous scaling analysis performed earlier [9, 10], a low-temperature DRACS test facility (LTDF) has been designed and constructed at OSU [8], as shown in Figs. 2 and 3. The LTDF uses water as the surrogate coolant for both the DRACS primary and secondary loops. The LTDF is intended to examine the couplings among the natural circulation/convection loops and provide us with experience that will be beneficial to the construction and operation of the high-temperature DRACS test facility (HTDF).

As shown in Fig. 2, the main components involved in the LTDF include a simulated core, DHX, NDHX, fluidic diode simulator, secondary throttling valve, pump, accumulator, air chimney system, and primary and secondary water tanks. The simulated core consists of a 4" Sch 80 (OD: 114.30 mm; ID: 97.18 mm) vessel made from type 304 stainless steel and three 1" (25.4 mm) diameter (D) cartridge heaters. The cartridge heaters are arranged in a triangular pattern with a pitch-to-diameter ratio (P/D) of 1.6 and wall distance-to-diameter (W/D) ratio of 1.4, respectively, as shown in Fig. 2(b). Each cartridge heater is capable of providing 2-kW power over a heated length of 1 m, with a total power of 6 kW from the core. There is an unheated length of 0.25 m at the heater end near the inlet of the simulated core vessel, mainly to provide a flow length for the flow to develop in the entrance region. Another unheated length of 0.1 m is added to the top of each heater's heated length to accommodate a plate spacer designed to align the three heaters. A J-type thermocouple is built into each of the heaters at the junction of the 0.1-m unheated

length and heated length to monitor the heater temperature and thus prevent overheating. During the operation, the surface temperature of the heaters could exceed 100°C, and to prevent any potential subcooled boiling, the primary loop and pump loop are pressurized to 1.0 MPa using a nitrogen-filled accumulator.



(a) Image of the LTDF



(b) Three-dimensional layout of the LTDF, its simulated core and fluidic diode simulator

Figure 2. An image and a three-dimensional layout of the LTDF

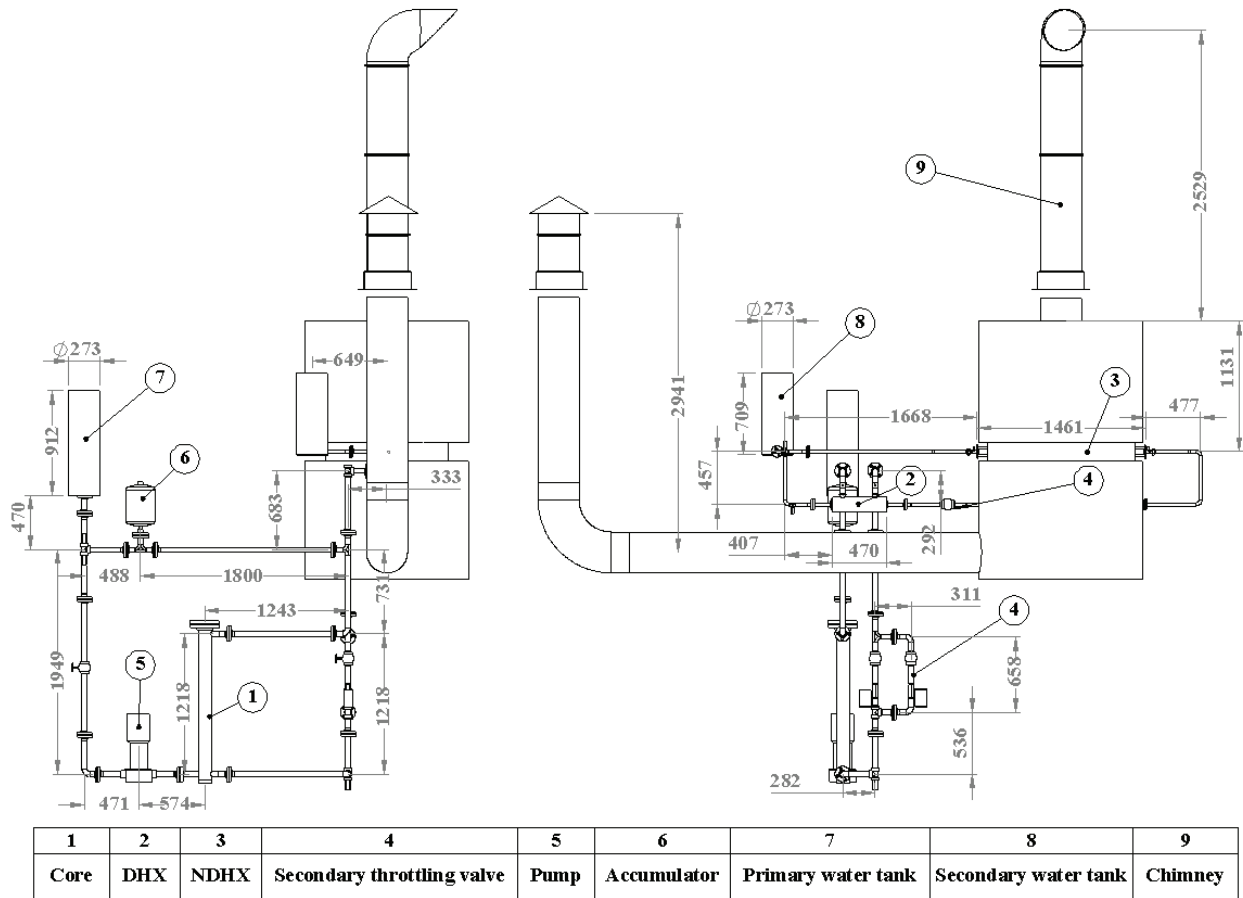


Figure 3. A two-dimensional as-built drawing of the LTDF (unit: mm)

A shell-and-tube heat exchanger with one tube pass is adopted for the DHX. The DHX employs 80 3/8" BWG-18 (OD: 9.53 mm; ID: 8.41 mm) tubes with a length of 0.356 m, all made from type 316 stainless steel. The tubes are arrayed in a triangular pattern with a pitch-to-diameter ratio of 1.208, and are contained in a shell with an inner diameter of 5 inch (127.0 mm). Four baffles with a baffle cut of 25.8% are used to support the tubes. In the DHX, the pressurized primary water flows on the shell side while the secondary water is on the tube side. For the NDHX, to enhance the air-side heat transfer, a finned-tube heat exchanger with copper tubes and aluminum fins has been employed. The NDHX contains 52 5/8" BWG-20 (OD: 15.88 mm; ID: 14.99 mm) finned tubes with a length of 0.99 m. These tubes are placed in two rows in a staggered array with a pitch-to-diameter ratio of 2.4. The fins are made from 12.07 mm tall and 0.254 mm thick circular aluminum plates, with a spacing of 10 fins/inch.

In the current LTDF, a combination of two globe valves and two ball valves is employed to simulate the fluidic diode, as shown in Fig. 2(b). The two parallel branches, each of which consists of a globe valve and a ball valve, simulate the forward and reverse flow directions of the fluidic diode. The two globe valves are identical, and can provide resistances as desired by turning the valve stem. The same globe valve is used as the secondary throttling valve to adjust the flow resistance in the secondary loop. The two ball valves are motorized, and only one of the two valves is open at a given flow direction.

A special air chimney design different from the prototypic concentric annular design [7, 10] has been adopted, as shown in Fig. 2. This is because the LTDF is built in a confined lab rather than an open space.

There are two 14" (355.6 mm) diameter penetrations on the roof of our lab, which are utilized as the entrance and exit of the chimney system. The NDHX, with a square face of 0.99 m by 0.99 m, is positioned between two big air ducts with an inner diameter of 1.41 m. All the indoor ducts are made from galvanized steel while the outdoor ducts above the roof are made from type 304 stainless steel. The smaller duct inside the room, as well as that at the exit, are insulated with a 1.5-inch (38.1 mm) thick fiberglass blanket to maintain the incoming air temperature and inhibit heat loss from the hot leg where the hot air rises after passing through the NDHX. The big ducts are insulated with a layer of 1-inch (25.4 mm) ceramic fiber blanket before applying the fiberglass blanket, mainly due to the high temperatures that will be encountered later in the high-temperature test facility since the air chimney ducts will be shared with the HTDF.

The LTDF includes a pump loop that simulates the intermediate heat transfer loop in an FHR. A 2-hp vertical inline circulating pump is employed in the pump loop, enabling the study of the flow reversal phenomenon in the DRACS primary loop following a pump trip event associated with loss of power and reactor shutdown. A variable frequency drive is used to control the speed of the pump. A 1-gallon bladder accumulator is also employed in the pump loop to pressurize the primary loop to 1.0 MPa. For safety concern, a relief valve with an adjustable set pressure between 1.0 to 2.0 MPa is employed in the primary loop at the DHX shell-side inlet. The primary and pump loops are built from 1-1/4" Sch 40 (OD: 42.16 mm; ID: 35.05 mm) type 304 stainless steel pipes, while the secondary loop is built from 3/4" Sch 40 (OD: 26.67 mm; ID: 20.93 mm) type 304 stainless steel pipes. The primary and pump loops are wrapped with 2-inch (50.8 mm) thick fiberglass insulation, and the secondary loop with 1.5-inch (38.1 mm) thick fiberglass insulation to reduce heat losses. Two water tanks are used to add water to the primary/pump and secondary loops, while the secondary water tanks also serves as the expansion tank.

Table I. Measurement errors of the instruments

Instrument	Vendor	Model #	Full Scale	Instrument Uncertainty
Ultrasonic Flow Meter	Flexim	ADM 7407	-0.4 to 0.4 m ³ /hr (primary loop) -0.2 to 0.2 m ³ /hr (secondary loop)	1% of reading + 9 mm/s
Thermal Mass Flow Meter	Eldridge	9840MPNH	0 to 1300 SCFM	1% of reading + (0.5% + 0.05%/°C) of full scale (ref: 21°C)
Differential Pressure Transducer	Honeywell	STD 120	0 to 250 Pa	0.0525% of full scale
Gauge Pressure Transducer	Honeywell	STD 140	0 to 2.0 MPa	0.075% of full scale
Thermocouple	Omega Engineering	TMQSS-125G-6	0 to 120°C (primary loop) 0 to 90°C (secondary loop) -20 to 60°C (air inlet) 0 to 200°C (air outlet)	0.5°C or 0.4% of full scale
Watt Transducer	Ohio Semitronics	PC5-117EY25	0 to 2000 W	0.5% of full scale

The LTDF is fully instrumented. Three clamp-on ultrasonic flow meters provided by Flexim, capable of measuring flows as small as 9 mm/s, are installed in the primary, pump, and secondary loops. A thermal

mass flow meter from Eldridge is employed for the air flow measurement in the air chimney, which employs a special averaging tube that reduces the required upstream straight pipe run and makes the measurement more accurate. The averaging tube employs several holes (facing upstream) to average the air velocity along the diameter of the air duct. A Honeywell STD 120 differential pressure transducer, with a minimum range of 0-250 Pa is used to measure the pressure drops over the fluidic diode simulator and secondary throttling valve, which are the main pressure drop contributors to their respective loops. A Honeywell STG 140 gauge pressure transducer, with a range of 0 to 2.0 MPa is used to monitor the pressure of the primary/pump loop when being pressurized. T-type thermocouples from Omega Engineering are employed to measure the inlet and outlet temperatures of all the heat exchange components, namely, the core, DHX, and NDHX. Lastly, each of the three core heaters is individually controlled by an SCR controller to adjust the power, and the actual power provide to each heater is measured by a watt transducer. All the instruments have been calibrated using standards whose accuracies are traceable to NIST (National Institute of Standards and Technology) and Table I lists the measurement errors of these instruments.

3. RESULTS AND DISCUSSIONS

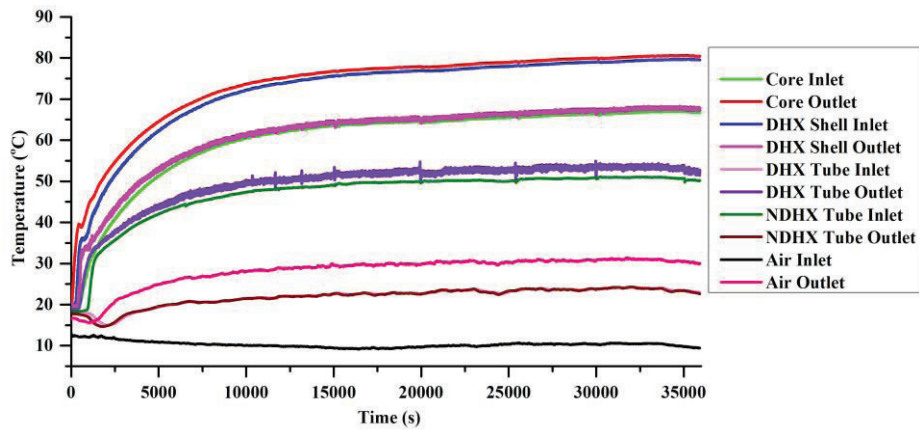
Two representative accident scenarios are simulated in the LTDF to demonstrate the capability and performance of the DRACS, with the results presented in detail in the following discussions.

3.1. Scenario 1

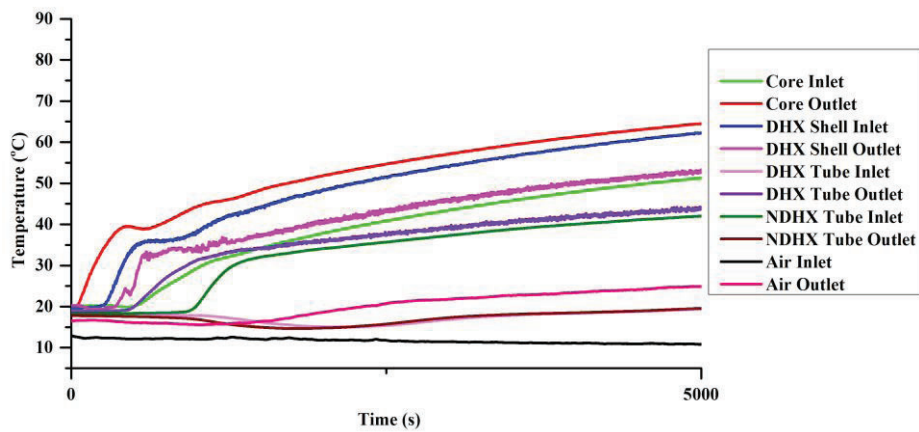
In Scenario 1, the accident transient is initiated with no initial flows in both the DRACS primary and secondary loops. A step change of power from 0 to 2.1 kW is triggered at time point of 0 through the SCR power controllers controlled by a program written in Labview. Before the power is turned on, the pump is turned on to circulate the primary water so that a nearly uniform temperature is obtained in the primary loop. The pump is subsequently turned off and the pump loop is isolated from the remaining of the LTDF by closing the globe valve in the pump loop. Without a pump in the secondary loop, a nearly uniform initial temperature is realized by flushing the loop with fresh water from the secondary water tank where the temperature is uniform. For the air loop, as will be seen in the following discussion, there is an initial temperature variance along the loop and correspondingly a non-zero initial flow, due to the heating induced by the temperature gradient from the secondary water (at the room temperature) to the ambient air (at the outside ambient temperature, lower than the room temperature at the time when the experiment is carried out). The initial temperatures and flow rates are controlled with care so that the initial conditions can be correctly characterized when the experimental data are used for future code validation/benchmarking.

The development of the coolant temperatures and flow rates following the initiation of the transient is shown in Figs. 4 and 5. As can be seen, natural circulation/convection is successfully developed in all three loops, and a steady state is reached at approximately 35,000 seconds. After the heater power is turned on, due to the relatively fast heat conduction through the heater sheath, the primary water in the core is heated up almost immediately, which is the reason why an immediate temperature increase is seen at the core outlet, as shown in Fig. 4(b). Because of this, buoyance also starts to build up in the primary loop from the beginning, leading to the development of the primary flow, as seen from Fig. 5(a). The heated primary water therefore flows toward the DHX, leading to subsequent temperature increases at the DHX shell-side inlet and outlet, and core inlet, as shown in Fig. 4(b). The secondary water starts being heated up when the hot primary water gets to the DHX shell-side inlet at approximately 300 seconds. However, as shown in Fig. 5(a), the secondary flow stays as almost zero until approximately 650 seconds. This is mainly because the DHX is located in the bottom horizontal leg in the secondary loop, and there is a horizontal section between the DHX tube-side outlet and the vertical leg, as can be seen from Figs. 2 and 3. Heat has to be transferred to the vertical leg through heat conduction in water, which is a slow

process, before the secondary flow starts to develop. For the air, as mentioned earlier, there is a small initial flow due to the heating by the secondary water, which can be seen from Fig. 5(b). This is the cause for the temperature decrease at the NDHX tube-side outlet, and subsequently the DHX tube-side inlet, as shown in Fig. 4(b). As the hot secondary water arrives at the NDHX tube-side inlet at approximately 1,000 seconds, the heat transferred to the air increases, causing an abrupt increase in the air flow rate, as seen from Fig. 5(b).

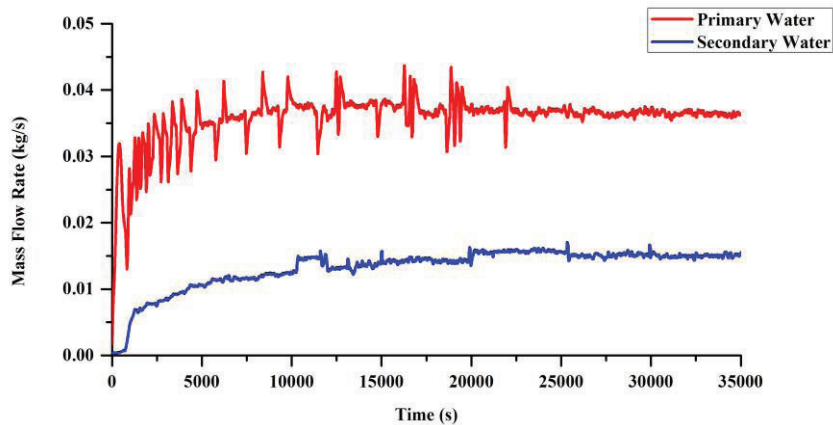


(a) Fluid temperature over 35,000 s (9.7 hours)

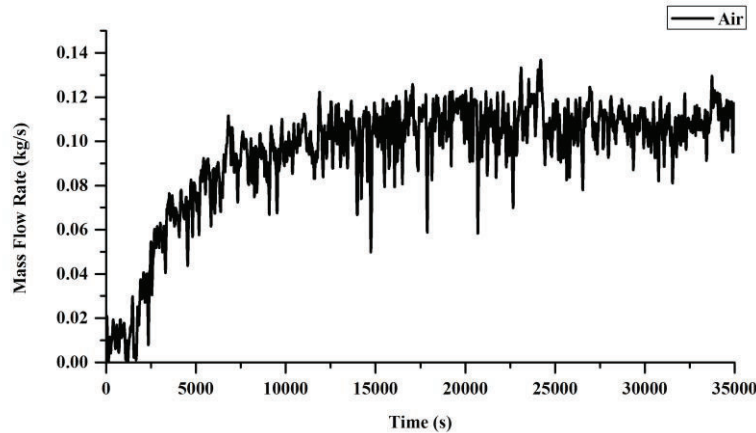


(b) Fluid temperature for the first 5,000 s

Figure 4. Fluid temperature evolution during the startup transient (a) over 35,000 s and (b) for the first 5,000 s



(a) Primary and secondary water



(b) Air

Figure 5. Mass flow rates during the startup transient for (a) primary and secondary water and (b) air

The conditions of the steady state reached near the end of the transient are summarized in Table II, along with the nominal conditions of the LTDF scientific design and the rating results of the as-built LTDF using the design code earlier developed for the LTDF. The LTDF design code is a one-dimensional code that solves the steady-state mass conservation equations, integral momentum equations, and energy balance equations for the three coupled natural circulation/convection loops [8, 11]. The fluids' temperatures and flow rates are coupled through the integral momentum equations and energy balance equations, and are solved for through an iteration process. The as-built LTDF differs from the scientific design mainly in the DHX and NDHX [8]. The rating process is based on the actual core operating power and air inlet temperature measured in the experiment, and assumes no heat loss. In a previous analysis, the total heat loss from the LTDF was estimated to be approximately 63 W, accounting for 3% of the total core power [12]. Uncertainties associated with the experimental results are analyzed using the root sum square method and are also given in Table II. The uncertainties include both the random uncertainties associated with the measurements and the systematic uncertainties associated with the instruments. The random uncertainties have been estimated to 95% confidence level. It is noted that the uncertainties of the flow rates are relatively big compared to the others. For the primary and secondary flow rates, this is

mainly due to the minimum uncertainty of 9 mm/s of the clamp-on ultrasonic flow meters that have been used. Actually, this minimum uncertainty is typical for all the industrial ultrasonic flow meters found so far. For the air flow rate, the uncertainty is mainly due to the random measurement uncertainty, which theoretically can be reduced by taking multiple measurements.

It should also be noted that, due to the heat loss along the pipes connecting the components of interest as well as the measurement uncertainties, there is a difference in temperature between the core outlet and DHX shell-side inlet, DHX shell-side outlet and core inlet, and so forth. The hot leg and cold leg temperatures of the primary and secondary loops, as well as the temperature differences given in Table II are averaged values over from 32,500 to 33,500 s. As can be seen from Table II, the experimental flow rates and temperature differences between the hot and cold sides match the rating results well, indicating that the loop height and flow resistance in each of the LTDF loops have been properly scaled. In the present experiment, the primary throttling valve in the fluidic diode simulator and the secondary throttling valve are opened to positions yielding flow coefficients of 5.25 and 20, respectively [8]. As can also be seen, the hot leg and cold leg temperatures of the secondary and air loops from the experiment match the rating results well, but not for the primary loop. This indicates that in the LTDF design code, the NDHX is correctly modeled, but the DHX is not. Another possible reason leading to the discrepancy could be the fouling resistance in the DHX, which is neglected in the LTDF design code. To find out the cause for the discrepancy, the DHX was taken apart from the LTDF and disassembled for an inspection. It was found that two tubes got rusted, causing rusty deposits onto the tubes and correspondingly the fouling resistances. In addition, it was noticed that the bottom 60% tubes on the tube side had noticeable rusty deposits while the top 40% tubes were relatively clean, indicating that the top 40% tubes were not covered with water (tube side) during the experiments. This was mainly due to the air being released and trapped in the DHX during the heating up of the secondary water (tube side), causing a loss of heat transfer area of almost 40%. These observations confirm the previous postulations. The DHX has been sent back to the vendor to replace the two rusted tubes, and air relief ports will be added to the DHX to release any air generated during the experiments.

Table II. Steady-state results and comparisons with the nominal LTDF design conditions and rating results of the as-built LTDF

Parameters	Design	Rating	Experiment
Power (W)	2,048	2,109	2,109 ± 21
Primary T_{hot} (°C)	76.5	65.1	79.5 ± 0.4
Primary T_{cold} (°C)	63.7	51.9	66.8 ± 0.4
Primary ΔT (°C)	12.8	13.2	12.7 ± 0.5
Primary Water Flow (kg/s)	0.0376	0.0381	0.0365 ± 0.0086
Secondary T_{hot} (°C)	65.2	54.1	52.2 ± 0.4
Secondary T_{cold} (°C)	34.8	23.1	24.0 ± 0.4
Secondary ΔT (°C)	30.4	31.0	28.3 ± 0.6
Secondary Water Flow (kg/s)	0.0161	0.0163	0.0150 ± 0.0034
Air T_{hot} (°C)	40	30.8	31.0 ± 0.5
Air T_{cold} (°C)	20	10.4	10.4 ± 0.6
Air ΔT (°C)	20	20.4	20.6 ± 0.8
Air Flow (kg/s)	0.102	0.103	0.103 ± 0.017

Table III. Heat balance results

	Heat Transfer Rate (W)
Watt Transducer Reading	2,109 ± 21
Core	2,112 ± 504
DHX Shell Side	1,823 ± 442
DHX Tube Side	1,864 ± 426
NDHX Tube Side	1,700 ± 388
NDHX Air Side	2,144 ± 360

A heat balance analysis has also been performed based on the steady-state results, as summarized in Table III. Due to the relatively large measurement uncertainties in the flow rates, large uncertainties are also encountered in the heat transfer rates due to the uncertainty propagation since the heat transfer coefficient is a function of the fluid mass flow rate. The implication learned here is that, for a natural circulation/convection system with small coolant flow rates, the large uncertainties in the measurements of the flow rates can cause large uncertainties in the heat balance calculations, making it difficult to quantify and model the heat loss. This issue will become more critical to any prototypic DRACS system, where heat loss would be significant due to the high temperatures of fluoride salts. Therefore, efforts in developing instruments capable of measuring small flows is deemed necessary.

3.1. Scenario 2

In Scenario 2, a steady-state core normal operation is first simulated before initiating the accident transient. This simulated core normal operation is different from the prototypic core normal operation in that there is no intermediate heat exchanger (IHX) in the LTDF. Therefore, the LTDF simulated core will not provide the nominal core power but instead a power representing the parasitic heat loss to the DRACS during core normal operation. For the simulated core normal operation, a constant power of 1.6 kW is provided to the LTDF core. The pump speed is adjusted in conjunction with the opening of the globe valve in the reverse flow direction of the fluidic diode simulator so that the parasitic flow through the fluidic diode and the main flow through the core are approximately 0.072 and 0.894 kg/s, respectively. The system is maintained in operation until a steady-state is reached, following which the accident is initiated by shutting down the pump and step increasing the core power to 2.1 kW that represents the decay heat. The initial parasitic flow through the fluidic diode simulator is constantly monitored, and when it decreases to zero, the branch representing the forward flow direction is opened and the other branch closed.

The evolution of the coolant temperatures and flow rates following the pump trip is shown in Figs. 6 and 7. As can be seen from Fig. 6, following the pump trip, temperatures in the primary loop experience an abrupt change due to the flow reversal, and then gradually approach a steady state. The flow reversal in the primary loop causes a small perturbation in the secondary loop temperatures (NDHX tube-side inlet and DHX tube-side outlet), which then decays away over a short period of time. After that, the secondary temperatures increase slowly until a new steady state is reached. No immediate effect of the pump trip or flow reversal is observed on the air temperatures. The same characteristics are observed on the secondary water flow rate and air flow rate, as shown in Fig. 7(a). It can be seen from Figs. 7(b) and 7(c) that, after the pump trip, the residual pump flow and the parasitic flow through the primary loop decrease to zero very quickly, mainly due to the large flow resistance in the loop and relatively small inertia of the pump. The primary water flow is seen to decrease to zero over approximately 3 seconds and start to develop in the reverse direction immediately. No significant period of time during which the primary flow is stagnant is observed during the flow reversal process, mainly due to the existing temperature gradient and

correspondingly buoyancy in the primary loop when the pump is shut down. Lastly, compared to the startup scenario discussed earlier, it takes much less time (~ 17,500 seconds) to reestablish the new steady state.

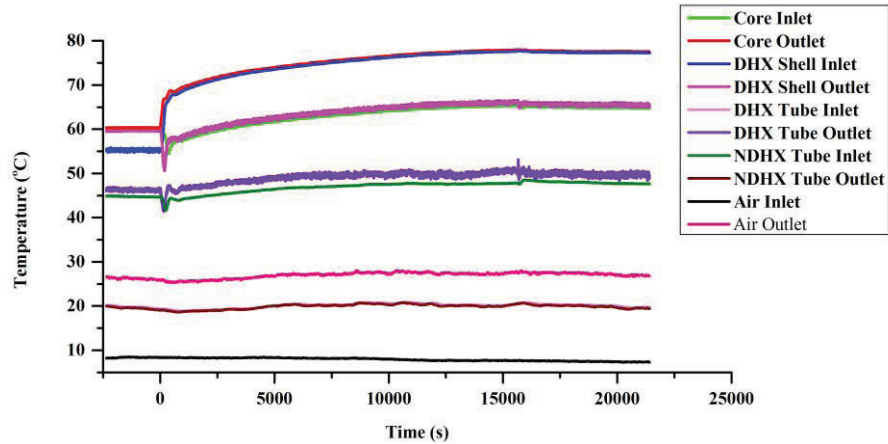
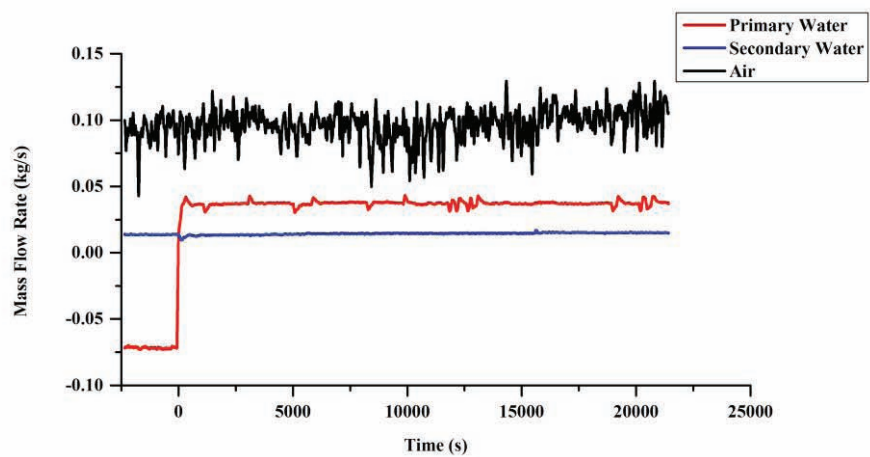
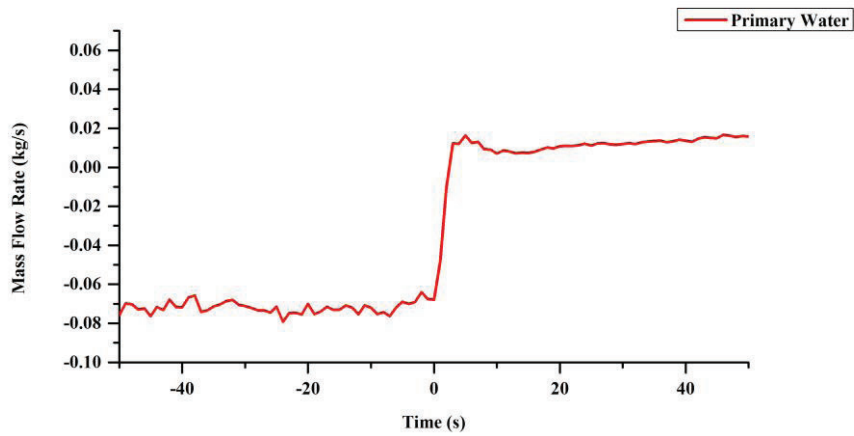


Figure 6. Fluid temperature development during the pump trip transient



(a)



(b)

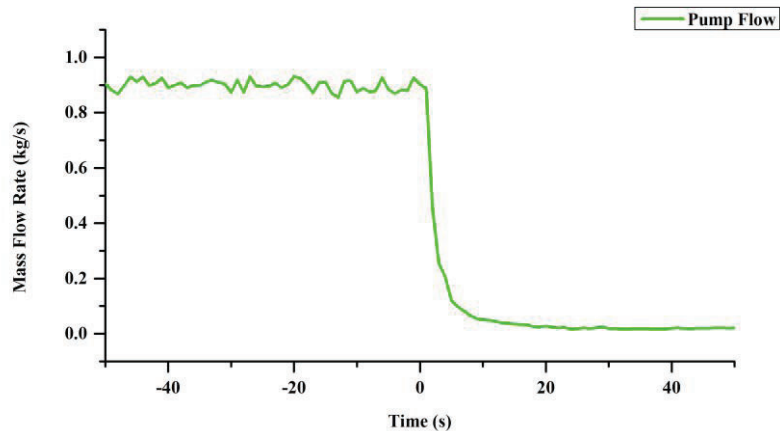


Figure 7. Mass flow rates during the pump trip transient

(c)

4. CONCLUSIONS

In the present paper, two accident scenarios, namely, the startup and pump trip events, are investigated using the LTDF. In both scenarios, natural circulations are successfully established, demonstrating the passive decay heat removal capability of the DRACS concept. The steady-state conditions reached in the startup scenario are compared with the system rating results obtained from the in-house LTDF design code, and show good agreement except for the primary loop temperatures. This discrepancy was caused by the loss of heat transfer area in the DHX due to the air released on the DHX tube side during the heating up of the secondary water, as well as the fouling resistance. In the pump trip scenario, the primary flow is found to reverse in about three seconds after the pump trip without any significant stagnation period during the reversal process. In addition, the pump trip transient lasts much shorter than that of the startup scenario. The functionality and heat removal capability of the DRACS concept are clearly demonstrated by these two experiments.

ACKNOWLEDGMENTS

This research was performed using funding received from the U.S. Department of Energy (DOE) Office of Nuclear Energy's Nuclear Energy University Programs. Dr. David Holcomb of the Oak Ridge National Laboratory provided valuable comments and is much appreciated.

REFERENCES

1. C.W. Forsberg, "The Advanced High-Temperature Reactor: High-Temperature Fuel, Liquid Salt Coolant, and Liquid-Metal-Reactor Plant," *Progress in Nuclear Energy*, **47** (1-4), pp. 32-43 (2005).
2. P. Bardet, E. Blandford, M. Fratoni, A. Niquille, E. Greenspan, and P.F. Peterson, "Design, Analysis and Development of the Modular PB-AHTR," *Proc. of ICAPP'08*, Anaheim, CA, June 8-12 (2008).
3. C.W. Forsberg, P. Pickard, and P.F. Peterson, "Molten-Salt-Cooled Advanced High-Temperature Reactor for Production of Hydrogen and Electricity," *Nuclear Technology*, **144**, pp. 289-302 (2003).
4. D.E. Holcomb, S.M. Cetiner, G.F. Flanagan, F.J. Peretz, and G.L. Yoder, "An Analysis of Testing Requirements for Fluoride Salt-cooled High Temperature Reactor Components," ORNL/TM-2009/297, Oak Ridge National Laboratory, Oak Ridge, TN, November (2009).
5. H. Zhang, H. Zhao, V. Mousseau, and R. Szilard, "Design Considerations for Economically Competitive Sodium Cooled Fast Reactors," *Proc. of ICAPP'09*, Tokyo, Japan, May 10-14 (2009).

6. C.W. Forsberg, L.W. Hu, P.F. Peterson, and K. Sridharan, "Fluoride-Salt-Cooled High-Temperature Reactor (FHR) for Power and Process Heat Final Project Report," MIT-ANP-TR-157, Massachusetts Institute of Technology, Cambridge, MA, December (2014).
7. X. Wang, Q. Lv, X. Sun, R.N. Christensen, T.E. Blue, G. Yoder, D. Wilson, and P. Sabharwall, "A Modular Design of a Direct Reactor Auxiliary Cooling System for AHTRs," *Transaction of the American Nuclear Society*, American Nuclear Society 2011 Annual Meeting, Hollywood, FL, June 26-30, Vol. 104, pp. 1077-1080 (2011).
8. Q. Lv, X. Wang, I. Adams, X. Sun, R.N. Christensen, T.E. Blue, G. Yoder, D. Wilson, and P. Sabharwall, "Design of a Scaled-down Low-temperature DRACS Test Facility for an AHTR," *Transaction of the American Nuclear Society*, American Nuclear Society 2012 Annual Meeting, Chicago, IL, June 24-28, Vol. 106, pp. 1071-1074 (2012).
9. Q. Lv, X. Wang, I. Adams, X. Sun, R.N. Christensen, T.E. Blue, G. Yoder, D. Wilson, and P. Sabharwall, "Scaling Analysis for the Direct Reactor Auxiliary Cooling System for AHTRs," *International Topical Meeting on Nuclear Reactor Thermal Hydraulics (NURETH-15)*, Pisa, Italy, May 12-17 (2013).
10. Q. Lv, X. Wang, I.H. Kim, X. Sun, R.N. Christensen, T.E. Blue, G. Yoder, D. Wilson, and P. Sabharwall, "Scaling Analysis for the Direct Reactor Auxiliary Cooling System for FHRs," *Nuclear Engineering and Design*, **285**, pp. 197-206 (2015).
11. Q. Lv, H.C. Lin, I.H. Kim, X. Sun, R.N. Christensen, T.E. Blue, G. Yoder, D. Wilson, and P. Sabharwall, "DRACS Thermal Performance Evaluation for FHR," *Annals of Nuclear Energy*, **77**, pp. 115-128 (2015).
12. Q. Lv, I. Adams, X. Wang, X. Sun, R.N. Christensen, T.E. Blue, G. Yoder, D. Wilson, and P. Sabharwall, "A MATLAB Code for Thermal Performance Evaluation of a Low-Temperature DRACS Test Facility," *Transaction of the American Nuclear Society*, American Nuclear Society 2012 Winter Meeting, San Diego, CA, November 11-15, Vol. 107, pp. 1374-1377 (2012).